# Numerical investigation of effect of fill ratio and inclination angle on a U-shaped elliptical gravity heat pipe thermal performance

*Yang Chen, Guofei Chen, Huijie Xu, and Jianqiu Zhou**

School of Energy Science and Engineering, Nanjing Tech University, Jiangsu 211816, China

* Corresponding author; E-mail: zhouj@njtech.edu.cn

**Abstract:**

As electronic devices become increasingly compact, effective thermal management is crucial for performance. This study establishes a model of a U-shaped elliptical gravity heat pipe with dual heating ends and a single cooling end. Through computational fluid dynamics (CFD) simulations, the impacts of filling ratio and inclination angle on the thermal transfer capacity for the heat pipe were investigated. The results indicate that the evaporator surface temperature and thermal resistance of the heat pipe initially decrease and then increase with an increasing filling ratio. Within the inclination range of 10° to 90°, the evaporator surface temperature and thermal resistance gradually decrease. The optimal filling ratio is found to be 65%, and the optimal inclination angle is 90°. Furthermore, it was observed that higher heat input intensifies the effects of filling ratio and inclination angle affecting heat pipe thermal performance. These findings highlight the critical role of these parameters in optimizing heat pipe performance under varying heat inputs.

Keywords: U-shaped elliptical gravity heat pipe; filling ratio; inclination angle;

## 1. Introduction

With the advent of the electronic information era, electronic devices are evolving towards miniaturization and integration. The thermal power of modern multi-core or multi-thread processors (CPUs) has reached levels between 250-300 W [1], with a heat flux density exceeding 10W/cm² [2]. In the realm of high-performance computing, the computing capacity and energy efficiency of servers have significantly improved, accompanied by an increasing thermal power consumption. This issue becomes particularly pronounced in multi-CPU servers, where heat dissipation challenges arise. Traditional cooling solutions typically allocate independent cooling systems to each CPU, which, although adequate for basic needs, presents considerable challenges in terms of space utilization and overall efficiency.

To optimize space utilization and enhance cooling efficiency, this study presents a dual-heated-end gravity heat pipe designed to consolidate the thermal output from two CPUs into a single heat sink. Compared to conventional heat pipes, this design employs a U-shaped

and elliptical cross-section, which effectively enhances heat transfer performance.

The thermal performance for gravity heat pipe is influenced by several key factors, including heating power, inclination angle, fill ratio, and internal working fluid. Previous studies have indicated that gravity heat pipes with high fill ratios exhibit superior heat transfer capabilities [2–4]. Li et al. [4] combined experimental and numerical simulation methods to demonstrate that, as heat input rises, the upper portion of the evaporator in low-filling-ratio heat pipes may experience overheating. Notably, gravity heat pipes with a 50% fill ratio achieved a minimum thermal resistance value of 0.0291 K/W and a maximum effective thermal conductivity of $3.75\times10^{4}$ $Wm^{-1}K^{-1}$ under 600W heating power. Kim et al. [5] discovered a thermosyphon inclined at 30° with a 50% fill ratio exhibited optimal thermodynamic performance under low heat flux conditions. Additional research has revealed significant variations in thermal resistance and temperature distribution depending on different inclination angles and fill ratios [6–9].

Moreover, the choice of operating fluid in heat pipes has a direct impact on their thermal transfer performance. Variations in the thermophysical properties of different fluids lead to significant differences in overall heat pipe performance [10]. Bandar Fadhl et al. [11] studied the internal thermal transfer and flow phenomena in heat pipes using R134a and R404a as working fluids, validating their results through simulations. Lu et al. [12] explored the effects of working fluids, including methanol, deionized water, and ethanol, on the thermal transfer characteristics of thermosyphons.

Besides these factors, geometric changes in heat pipes also significantly influence their thermal performance. Research indicates that flat cross-sectional heat pipes outperform their circular counterparts [13,14], and the incorporation of internal fins can markedly improve heat transfer efficiency [15]. Elliptical cross-section heat pipes have demonstrated superior thermal capabilities across multiple studies [16–19].

Based on the current body of research, investigations into gravity heat pipes primarily focus on the impacts of filling ratio, working fluid, thermal input, and inclination angle on thermal transfer characteristics. However, geometric variations also significantly influence thermal performance. Therefore, this study introduces a U-shaped gravity heat pipe featuring an elliptical cross-section and examines its internal heat transfer flow characteristics.

## 2. Model description

### 2.1. Physical model

In this study, modelling software was utilized to generate the geometric model for the heat pipe. The thermal transfer in this heat pipe occurs via the evaporation and condensation processes of the operating fluid, as illustrated in Fig. 1-(a). Water is employed as the operating fluid in the heat pipe. The heat pipe is constructed from copper with a wall thickness of 0.9 mm. The entire heat pipe is divided into five sections: two evaporation sections, two adiabatic sections, and one condensation section. The lengths of these sections are as follows: the evaporation section has a length of 60 mm, the adiabatic section has a length of 20mm, and the condensation section also has a length of 20 mm. The condensation portion is chilled using water for the heat pipe. The heat pipe has an elliptical cross-section. The geometric

model of the heat pipe is presented in Fig. 1-(b).

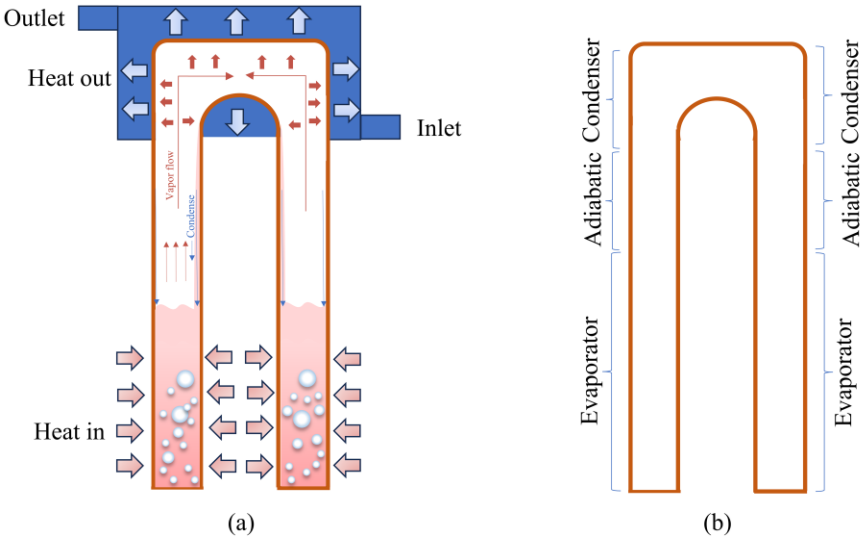


**Fig 1. Schematic of the heat pipe working principle and geometric model.**

## 2.2. Mathematic model

The Volume of Fluid (VOF) model was employed in the present study to model the evaporation and condensation heat transfer inside the heat pipe. This model can accurately capture the interface between the liquid and vapor phases and continuously update the gas-liquid interface by calculating the spatial volume distribution of different flow phases. Given the simultaneous occurrence of condensation and boiling within the heat pipe, the VOF method is utilized for simulating the two-phase flow inside the heat pipe and visualizing the internal flow behavior. The CFD model was established using ANSYS Fluent software utilizing the VOF method.

Each cell within the simulation domain consists of either one phase or a mixture of two phases, with the potential states of each phase is listed as shown below:

When $\alpha_l$ =1, the cell is completely filled with the liquid phase.

When $\alpha_l$ =0, the cell is entirely filled with the vapor phase.

When 0<$\alpha_l$<1, The cell consists of a liquid-vapor mixture.

### *2.2.1. Governing Equations*

(1) Continuity Equation:

$$\frac{\partial}{\partial t}\left(\alpha_l \rho_l\right)+\nabla\cdot\left(\alpha_l \rho_l \vec{u}_l\right)=S_M \tag{1}$$

Where $\rho$ represents the density (kg/m³), $\alpha$ denotes the volume fraction, and $\vec{u}$ is the velocity vector of the fluid. The subscript $l$ indicates the liquid phase. $S_M$ is the mass transfer source term at the gas-liquid interface, which quantifies the transfer of mass between phases during evaporation and condensation.

(2) Momentum Equation:

$$\frac{\partial}{\partial t}\left(\rho\vec{u}\right)+\nabla\cdot\left(\rho\vec{u}\vec{u}\right)=-\nabla P+\nabla\cdot\left[\mu\left(\nabla\vec{u}+\nabla\vec{u}^{T}\right)\right]+\rho\vec{g}+\vec{F} \tag{2}$$

$$\mu = \alpha_l \mu_l + \alpha_v \mu_v \tag{3}$$

$$\rho = \alpha_l \rho_l + \alpha_v \rho_v \tag{4}$$

Where $g$ represents the gravitational acceleration, $\mu$ denotes the dynamic viscosity, $P$ indicates the pressure, and $F$ represents the external forces exerted upon the fluid. In the VOF model, the physical characteristics of the mixture are defined by the volume fractions of the liquid and vapor phases.

In the practical application of the momentum equation, the effects of surface tension are often considered. Therefore, a continuous surface tension model is incorporated into the momentum equation [20].

$$F_{CFS} = \sigma \frac{\alpha_l \rho_l \kappa_l \nabla \alpha_l + \alpha_v \rho_v \kappa_v \nabla \alpha_v}{0.5\left(\rho_l + \rho_v\right)} \tag{5}$$

Where $\kappa$ represents the interface curvature, which can be determined using the subsequent formula:

$$\kappa_l = -\kappa_v = \nabla\left(\frac{\nabla \alpha_l}{\left|\nabla \alpha_l\right|}\right) \tag{6}$$

(3) Energy Equation:

$$\frac{\partial}{\partial t}\left(\rho E\right) + \nabla \cdot \left[\vec{u}\left(\rho E + P\right)\right] = \nabla \cdot \left(\lambda \nabla T\right) + S_E \tag{7}$$

In the equation, $S_E$ denotes the energy source term that encompasses the influences of evaporation and condensation, $\lambda$ indicates the volume-averaged thermal conductivity, $T$ is the temperature, and $E$ is the enthalpy. Both $T$ and $E$ are mass-averaged variables. The values of $\lambda$ and $E$ can be computed using the subsequent formulas:

$$E = \frac{\alpha_l \rho_l E_l + \alpha_v \rho_v E_v}{\alpha_l \rho_l + \alpha_v \rho_v} \tag{8}$$

$$\lambda = \alpha_l \lambda_l + \alpha_v \lambda_v \tag{9}$$

In the equations, $E_l$ and $E_v$ are calculated dependent on the specific heat capacities ($C_p$) of the respective phases and the temperature. The calculation formulas are as follows:

$$E_l = c_{p,l}(T - T_{sat}) \tag{10}$$

$$E_v = c_{p,v}(T - T_{sat}) \tag{11}$$

Where $c_{p,l}$ and $c_{p,v}$ represent the specific heat capacities for the liquid phase and vapor phase, respectively.

(4) Phase Change Equation:

The phase transition across liquid and vapor is essential for thermal transfer in gravity heat pipes. Therefore, a precise phase transition model is also essential for the entire simulation process. During the heat pipe simulation process, the Lee model presents certain issues [21-23]. Previous researchers have addressed this by using User Defined Function

(UDF) [2,4] or modified versions of the Lee model [24,25] for heat pipe simulations. Therefore, UDF is used to perform Fluent calculations, avoiding the inaccuracies associated with the Lee model. Essentially, this UDF calculates the mass and thermal transfer during the boiling and condensation processes. The equations describing the source terms related to boiling and condensation are as follows:

Evaporation $T_{mix}>T_{sat}$

Liquid phase:

$$S_M = -0.1\alpha_l\rho_l\left|\frac{T_{mix}-T_{sat}}{T_{sat}}\right| \tag{12}$$

Vapor phase:

$$S_M = 0.1\alpha_l\rho_l\left|\frac{T_{mix}-T_{sat}}{T_{sat}}\right| \tag{13}$$

Similar to the evaporation process, the expression for the condensation process is as follows:

Condensation $T_{mix}<T_{sat}$

Liquid phase:

$$S_M = 0.1\alpha_v\rho_v\left|\frac{T_{mix}-T_{sat}}{T_{sat}}\right| \tag{14}$$

Vapor phase:

$$S_M = -0.1\alpha_v\rho_v\left|\frac{T_{mix}-T_{sat}}{T_{sat}}\right| \tag{15}$$

In the energy equation, the energy source term $S_E$, which represents the thermal transfer due to phase transition, is determined by the mass source term and can be represented in the following manner:

Evaporation:

$$S_E = -0.1\alpha_l\rho_l\left|\frac{T_{mix}-T_{sat}}{T_{sat}}\right|LH \tag{16}$$

Condensation:

$$S_E = 0.1\alpha_v\rho_v\left|\frac{T_{mix}-T_{sat}}{T_{sat}}\right|LH \tag{17}$$

$T_{mix}$ and $T_{sat}$ denote the temperature of the mixture and the saturation temperature, respectively, and $LH$ is the latent heat of the working medium. A single source term for both phases is necessary in the calculation of heat transfer during evaporation or condensation.

### 2.3. Solution condition and solution strategy

All cases are solved using the pressure solver in ANSYS Fluent. A fixed time step of $10^{-4}$ is set throughout the solving process. To shorten computation time, the initial

temperature of the heat pipe is set to the saturation temperature of 373.15 K. The inlet water flow velocity at the condenser portion of the heat pipe is set to 0.05 m/s, with a temperature of 300 K. UDF is employed to replace the Lee model for solving the mass and energy source terms during the phase transition process of the heat pipe. For the two-phase operating fluid, the vapor phase is treated as an ideal gas. In the VOF model, the primary phase is the liquid phase, while the secondary phase is the vapor phase. The density of liquid water is defined as a polynomial that varies with temperature [26]. The overall flow regime is selected as laminar. Pressure-velocity coupling is computed using the SIMPLE algorithm. Additionally, the energy, momentum, and density equations are solved using the second-order upwind scheme, while pressure calculations utilize the PRESTO! method. The volume fraction is captured using the Geo-Reconstruction method to delineate the liquid-vapor interface. In this study, numerical convergence is achieved when the scaled residuals for the mass, velocity, and energy equations are less than $10^{-4}$, $10^{-6}$, and $10^{-12}$, respectively.

## 3. Results and discussion

### 3.1. Numerical simulation validation

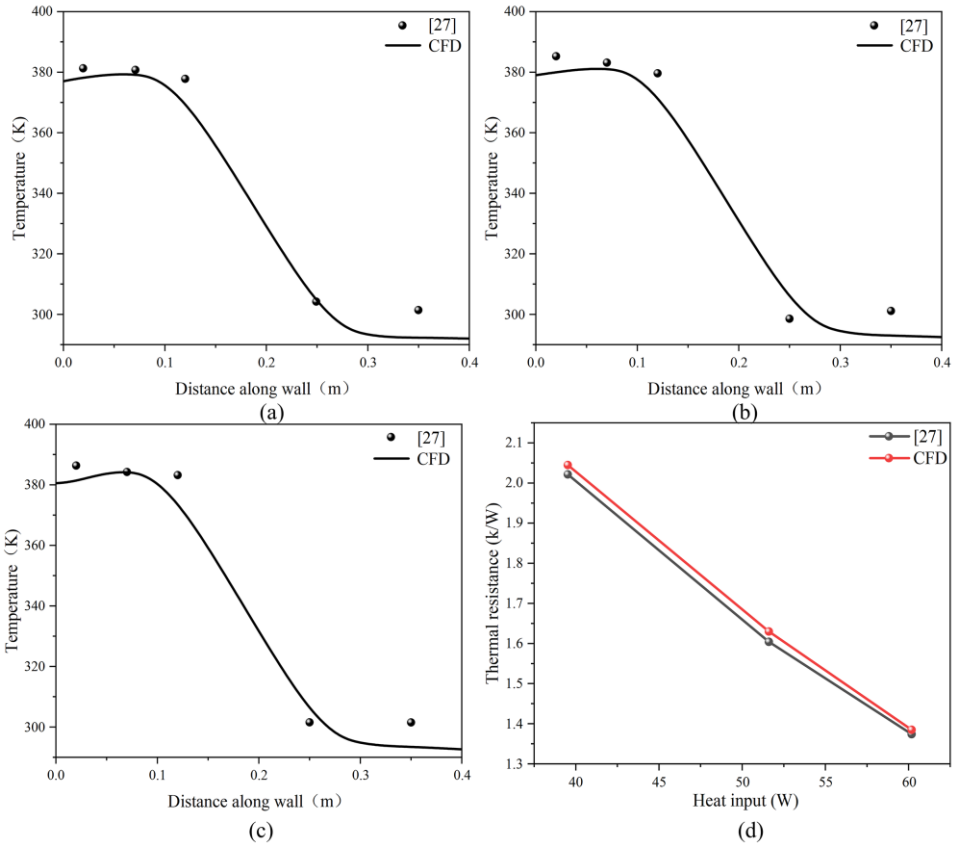


**Fig. 2 Comparison of heat pipe temperature and thermal resistance variations between literature data and CFD results.**

To confirm the accuracy of the CFD simulation, the operating parameters are the same for the model and experiment [27]. Fig. 2(a-c) shows the surface temperature differences between the CFD simulation results and experimental data at 39W, 50W, and 60W. Fig. 2(a-c)

presents the comparison of thermal resistance between the CFD simulation results and experimental data under power levels of 39 W, 50 W, and 60 W. These results indicate that the overall trend of the simulation aligns well with the experimental results, with a maximum error of 3.1%. Therefore, the model is considered reliable. Additionally, this study performed a Pearson correlation analysis on the data from the four images mentioned above. The formula for calculating the Pearson correlation coefficient is as follows:

$$r = \frac{\sum_{i=1}^{n}\left(x_i - \bar{x}\right)\left(y_i - \bar{y}\right)}{\sqrt{\sum_{i=1}^{n}\left(x_i - \bar{x}\right)^2}\sqrt{\sum_{i=1}^{n}\left(y_i - \bar{y}\right)^2}} \tag{18}$$

The variables $x$ and $y$ represent the experimental values from the literature and the CFD results obtained in this study, respectively. The correlation coefficient ($r$), ranging from -1 to 1, quantifies the strength of the linear relationship between the two datasets, with larger values of r indicating stronger correlations and higher reliability of the model. The calculated correlation coefficients for the experimental and simulated data in the four figures are 0.9957, 0.9910, 0.9920, and 0.9998, respectively. These results demonstrate a strong linear correlation between the experimental and simulated data, further validating the accuracy of the proposed model.

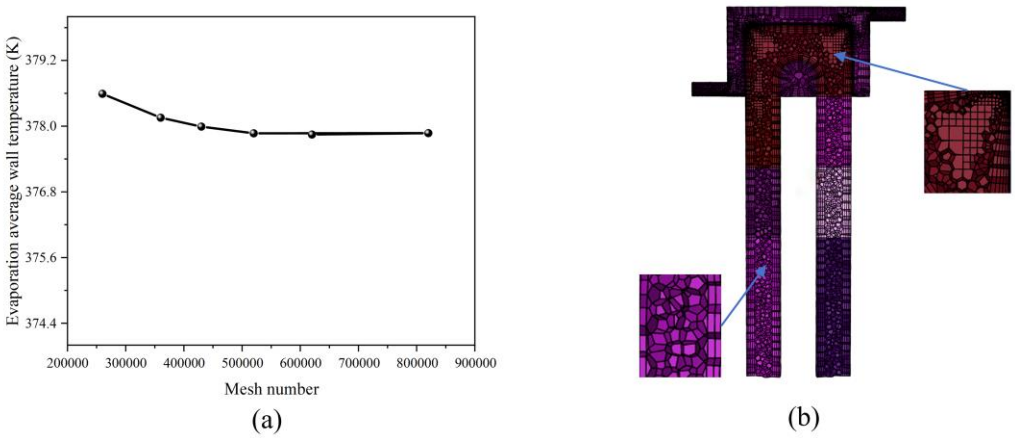


**Fig. 3 Grid independence verification and mesh model.**

To improve the accuracy of the numerical simulation, this study adjusted the local grid density at the boundaries of the evaporation and condensation sections to validate grid independence. Additionally, the temperature of the evaporation section under different mesh densities was compared, as shown in Fig. 3-(a). The comparison reveals that when the number of mesh elements exceeds 620,742, the mesh density has negligible impact on the simulation results. The mesh model is depicted in Fig. 3-(b). Therefore, in subsequent studies, the number of mesh elements for the model is maintained at approximately 620 thousand.

### 3.2. Effect of fill ratio

In this study, CFD simulations were used to study the impact of filling ratio for the heat pipe's heat transfer performance. The temperature contour of the heat pipe at 100 W and 65% filling ratio is illustrated in Fig. 4. Due to the steady heat flux applied at the evaporator region of the heat pipe, the operating fluid inside the pipe absorbs the heat extracted from the

evaporator. The temperature of the operating fluid rises continuously until it reaches the saturation temperature, at which point phase change occurs, and high-temperature vapor rises. The temperature at the upper portion of the heat pipe increases steadily until it reaches a stable state.

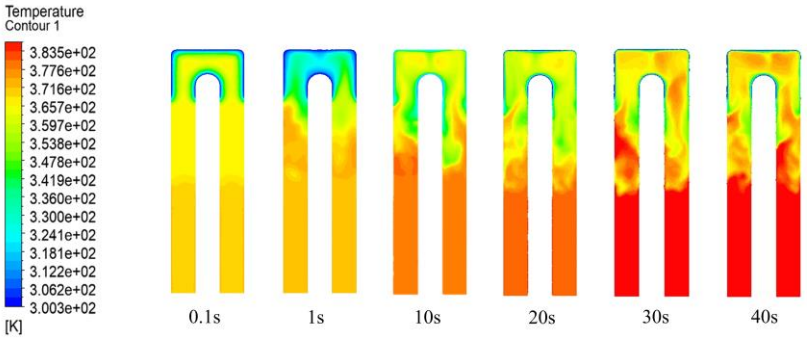


**Fig. 4 Temperature distribution at different times (65%, 100W).**

The change of vapor volume fraction with time is illustrated in Fig. 5. Initially, the bubbles exhibit a relatively small size. As the simulation time progresses and the operating fluid temperature rises, the volume and number of bubbles increase continuously, reaching a stable state at 40 seconds.

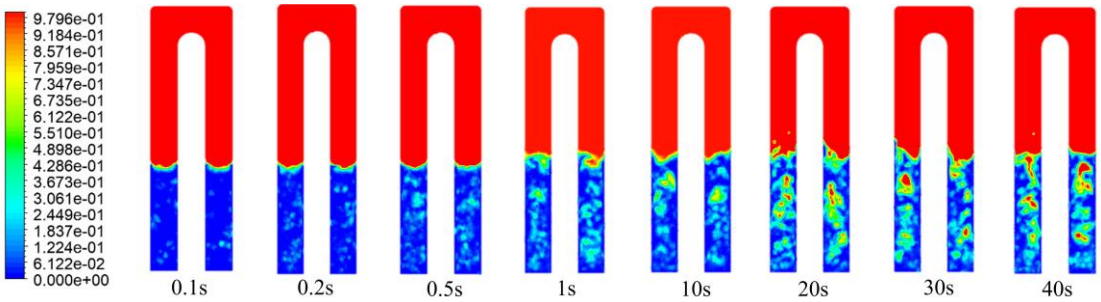


**Fig. 5 Vapor volume fraction distribution at different times (65%, 100W).**

Fig. 6 illustrates the outer wall temperature distribution of the heat pipe at filling ratios of 45%, 55%, 65%, and 75% under thermal inputs of 50 W, 80 W, and 100 W, respectively. Fig. 6 shows that the temperature distribution along the lower part of the heat pipe exhibits a similar trend under different filling ratios for the three heat input conditions. It is also noted that changing the thermal input and filling ratio has a greater impact on the temperature distribution in the evaporator than in the condenser. Moreover, under all heat input conditions, the wall temperature distribution is lowest when the filling ratio is 65%. In contrast, wall temperatures are higher at filling ratios of 45% and 55% under all heat input conditions. As the thermal input rises, the temperature rise becomes more pronounced, reaching a maximum at a thermal input of 100 W and a filling ratio of 45%. When the filling ratio is 75%, the surface temperature of the heat pipe does not decrease with the rise in the filling ratio. The surface temperature of the heat pipe at a 75% filling ratio is slightly elevated compared to the 65% filling ratio. This is due to more liquid in the evaporator, making it harder for large bubbles to rise to the surface of the liquid. Large bubbles that are unable to contact the liquid surface generate a vapor film adhering to the inner surface of the evaporator, resulting in a rise in temperature in that area. Therefore, the surface temperature of the heat pipe at a 75% filling ratio is slightly elevated in comparison to the 65% filling ratio.

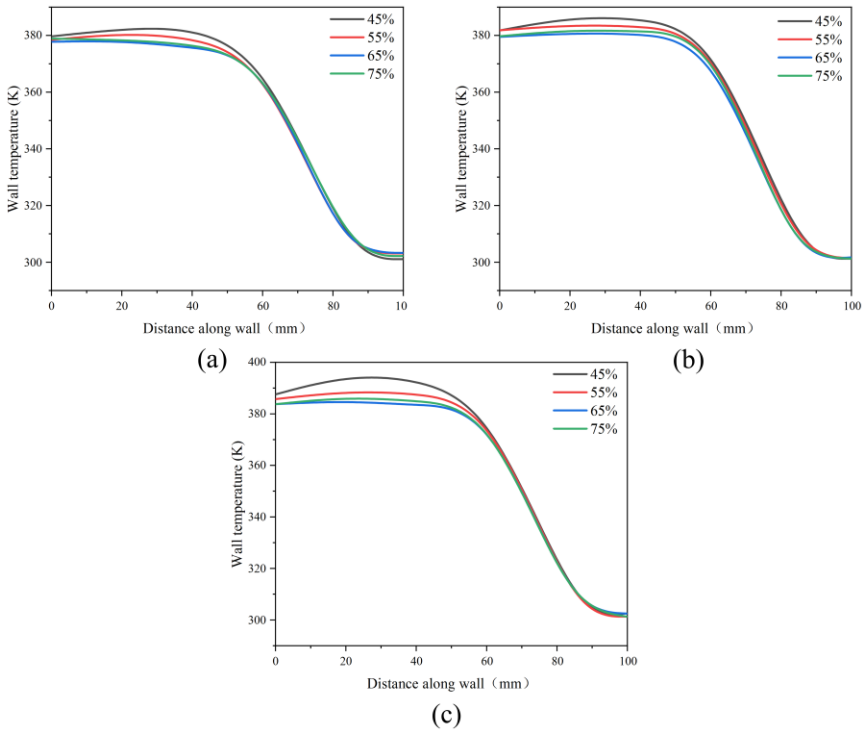


**Fig. 6 Temperature variation of the heat pipe at various thermal inputs for different filling ratios (a:50W; b:80W; c:100W).**

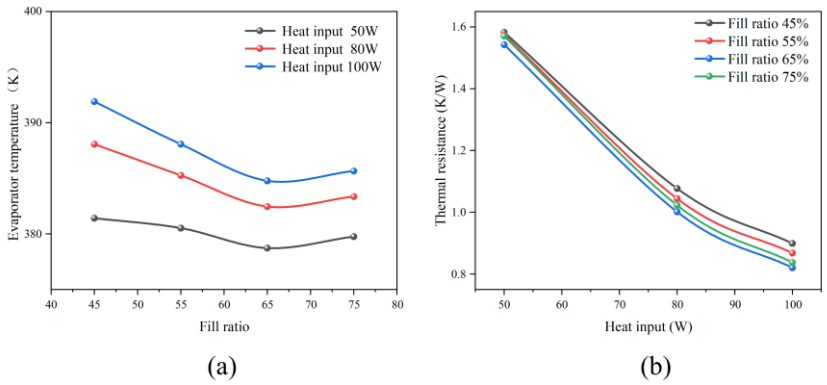


**Fig. 7 Change in average surface temperature of the evaporator based on fill ratio across various thermal inputs and change in thermal resistance in relation to thermal inputs at various fill ratios.**

Fig. 7-(a) depicts how the filling ratio affects the mean surface temperature of the evaporator across three different thermal input scenarios. The findings show that the evaporator temperature declines from the highest wall temperature at a 45% filling ratio to the lowest at 65%, and then shows an upward trend as the filling ratio increases to 75%. When the thermal input is 50 W, the variation in wall temperature of evaporator among different filling ratios is relatively small. However, when the thermal input is 80 W and 100 W, the variation in wall temperature becomes more pronounced compared to that at 50 W. Therefore, the influence of the filling ratio on the evaporator surface temperature is greater under comparatively high heat input conditions.

Fig. 7-(b) demonstrates how heat input influences thermal resistance at different filling ratios. Overall, the heat pipe thermal resistance declines with enhancing thermal input for all

filling ratios. Due to the low liquid volume, the thermal resistance is relatively high at a 45% filling ratio, whereas it is lower at a 65% filling ratio under different heat input conditions. However, compared to high heat input conditions, The variation in thermal resistance among heat pipes with different filling ratios is relatively minor at a heat input of 50 W. When the thermal input increases to 80 W and 100 W, the thermal resistance of the heat pipe with a 45% filling ratio shows a larger deviation compared to other filling ratios. This phenomenon occurs because, under low heat input conditions, heat pipes with various filling ratios can operate stably to achieve heat transfer. However, under high thermal input conditions, heat pipes with low filling ratios reach their thermal transfer limit, resulting in higher evaporator temperatures and greater differences in thermal resistance. Additionally, at filling ratios of 45%–65%, the thermal resistance of the heat pipe decreases as filling ratio enhances under all three heat input conditions. However, at filling ratios of 65%–75%, the thermal resistance increases as the filling ratio rises. This is because of the excessive liquid elevation, which prevents bubbles from approaching the liquid surface to transport thermal upwards. Bubbles form a vapor film on the pipe wall, rising the evaporator temperature and, consequently, the thermal resistance. Hence, the optimal filling ratio is around 65%.

### 3.3. Effect of inclination angle

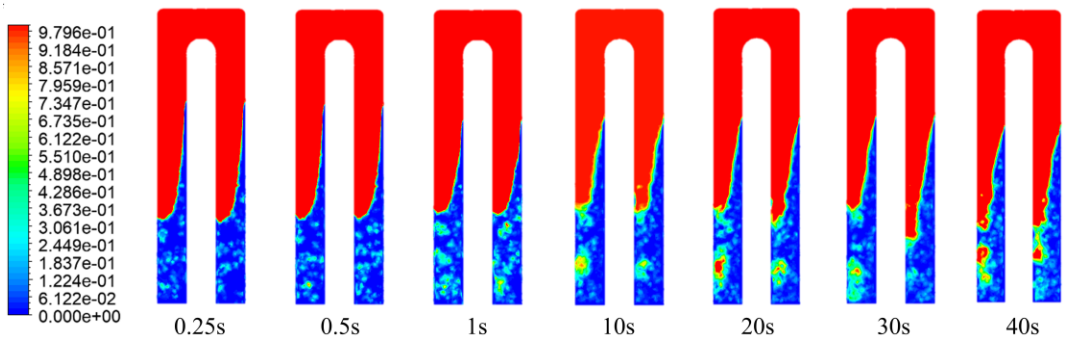


**Fig. 8 Vapor volume fraction distribution at different times for inclination angle 10°(65%, 100W).**

This work employs CFD simulations in studying the capability of the heat pipe at inclinations of 10°, 30°, 50°, 70°, and 90°, focusing on the role of inclination angle in heat pipe performance. Fig. 9 shows the variation of vapor volume fraction inside the heat pipe at an inclination angle of 10°, a thermal input of 100 W, and a filling ratio of 65%. Because of the inclination of the heat pipe, the liquid elevation within the evaporator is asymmetrical, causing certain areas of the evaporator wall do not come into contact with the working fluid. This prevents heat from being transferred effectively from these sections of the wall, resulting in elevated wall temperatures. Additionally, it is noted that the size of the bubbles stays relatively small. This is because the bubble nucleation sites on the liquid surface are closer to the pipe wall, reducing the distance between the bubbles and the liquid surface. As a result, small bubbles leave the liquid surface before growing into larger bubbles, thereby maintaining a smaller bubble size.

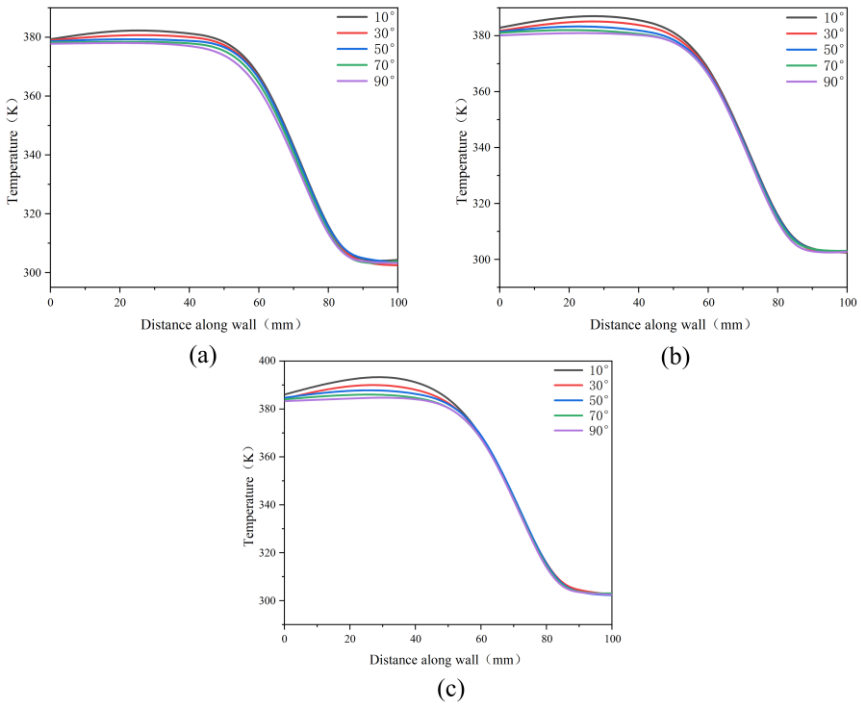


**Fig. 9 Variation of temperature of the heat pipe at different heat input for different inclination angles (a:50W; b:80W; c:100W).**

Fig. 9 illustrates the change in surface temperature along the length of the heat pipe for three various thermal inputs and multiple inclination angles. The overall trend in wall temperature is similar for the three heat input conditions, with the maximum and minimum wall temperatures occurring at 10° and 90°, respectively. Moreover, as the thermal input rises, the temperature disparity between the highest and lowest wall temperatures also widens. As the inclination angle declines, certain areas of the evaporator wall do not come into contact with the working fluid, preventing effective thermal transfer. Additionally, due to the inclination, bubbles rising from the lower wall to the upper wall of the evaporator cannot leave the liquid surface in a timely manner. The accumulated bubbles form large bubbles on the upper wall, reducing the thermal transfer efficiency between the upper wall and the operating fluid and causing thermal accumulation. With higher thermal input levels, the amount of heat accumulation also increases, exacerbating the negative impact of the inclination angle on the heat pipe. Therefore, the effect of inclination angle becomes more pronounced with increasing heat input.

Fig. 10-(a) illustrates how the inclination angle affects the evaporator surface temperature at different heat input settings. It can be seen that under varying thermal inputs, the evaporator surface temperature decreases in response to increasing inclination angle. The higher the heat input, the greater the variation in evaporator temperature, indicating that the impact of inclination angle on the heat pipe becomes more significant with rising thermal input.

Fig. 10-(b) illustrates the impact of inclination angle upon thermal resistance across different thermal input conditions. It can be noticed that thermal resistance gradually diminishes with the rise in inclination angle, reaching its minimum value at 90°. Under all three heat input conditions, the maximum and minimum thermal resistance occur at 10° and

90°, respectively.

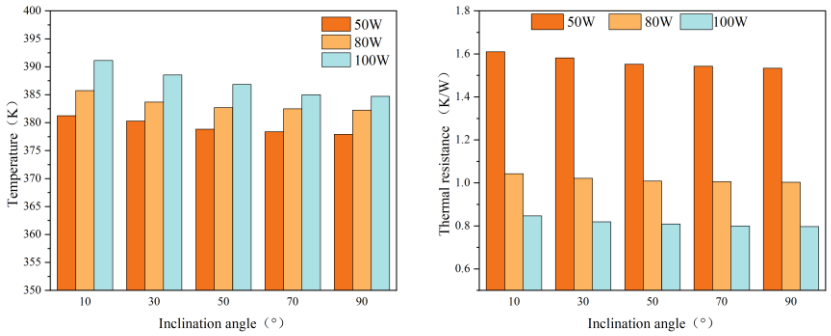


(a) (b)

**Fig.10 Change in the evaporator wall temperature with respect to inclination angle and change in thermal resistance as a function of inclination angle.**

## 4. Conclusion

This study compares the performance of a U-shaped elliptical gravity heat pipe with four different filling ratios (45%, 55%, 65%, and 75%) and five inclination angles (10°, 30°, 50°, 70°, and 90°) using CFD simulations. An investigation was conducted on how filling ratio and inclination angle affect heat pipe performance. The results indicate that:

- The filling ratio and inclination angle significantly affect the thermal transfer capability of the heat pipe. Under three different heat input conditions (50 W, 80 W, and 100 W), the evaporator surface temperature and thermal resistance first decline and then rise with growing filling ratio. The evaporator wall temperature and thermal resistance decline continuously with increasing inclination angle and reach a minimum at 90°.
- The optimal filling ratio and inclination angle for the heat pipe are 65% and 90°, respectively.
- Additionally, as the thermal input rises, the influence of the filling ratio and inclination angle on the heat pipe becomes more pronounced. The evaporator surface temperature of the optimal filling ratio is 2.86 K, 5.61 K, and 7.13 K lower than that of the low filling ratio heat pipe, and the thermal resistance decreases by 2.5%, 7.1%, and 9.6%, respectively. When the inclination angle rises from 10° to 90°, the evaporator temperature declines by 3.32 K, 4.51 K, and 7.12 K under three different power levels, and the thermal resistance declines by 3.3%, 5.3%, and 7.1%.

## Nomenclature

| | | | |
|---|---|---|---|
| $C_p$ | -specific heat, $Jkg^{-1}K^{-1}$ | *Greek symbols* | |
| $E$ | -total energy per unit mass, $Jkg^{-1}$ | $\alpha$ | -volume fraction |
| $F$ | -external force, N | $\mu$ | -dynamic viscosity, $Nsm^2$ |
| $F_{CFS}$ | -Continuum surface force | $\rho$ | -density, $[kgm^{-3}]$ |
| $g$ | -Gravity, $[ms^{-2}]$ | $\sigma$ | -surface tension, $[Nm^{-1}]$ |
| $K$ | -surface curvature | $\lambda$ | -thermal conductivity, $[Wm^{-1}K^{-1}]$ |
| $LH$ | -latent heat, $[Jkg^{-1}]$ | | |

| | | | |
|---|---|---|---|
| $P$ | -pressure, [Pa] | *Subscripts* | |
| $\vec{u}$ | -velocity vector, [$ms^{-1}$] | $l$ | -liquid |
| $S_E$ | -Energy transfer source term | $v$ | -vapor |
| $S_M$ | -mass transfer source term | $E$ | -Energy |
| $T$ | -temperature, [K] | $M$ | -Mass |
| $t$ | -Time, [s] | $mix$ | -mixture |
| | | $sat$ | -saturation |

**References**


[1] Du, S., et al., Simulation analysis on energy consumption and economy of CPU cooling system based on loop heat pipe for data center[J]. *Thermal Science and Engineering Progress*, 45(2023), 102115.

[2] Wang, K., et al. Numerical simulation on the heat transfer characteristics of two-phase loop thermosyphon with high filling ratios[J]. *International Journal of Heat and Mass Transfer*, 184(2022), 122311.

[3] Alammar, A. A., et al., Effect of inclination angle and fill ratio on geyser boiling phenomena in a two-phase closed thermosiphon – Experimental investigation[J]. *Energy Conversion and Management*, 156(2018), pp. 150-166.

[4] Li, G., et al. Transient experimental and numerical study of thermosyphon under different heating fluxes and filling ratios[J]. *Applied Thermal Engineering*, 243(2024), 122514.

[5] Kim, Y., et al., Boiling and condensation heat transfer of inclined two-phase closed thermosyphon with various filling ratios[J]. *Applied Thermal Engineering*, 145(2018), pp. 328-342.

[6] Alammar, A. A., et al., Numerical investigation of effect of fill ratio and inclination angle on a thermosiphon heat pipe thermal performance[J]. *Applied Thermal Engineering*, 108(2016), pp. 1055-1065.

[7] Xu, Z., et al., The influences of the inclination angle and evaporator wettability on the heat performance of a thermosyphon by simulation and experiment[J]. *International Journal of Heat and Mass Transfer*, 116(2018), pp. 675-684.

[8] Anto, L. P., Varghese, J., Three-dimensional steady state numerical analysis of inclined two phase closed thermosyphon for solar applications[J]. *Case Studies in Thermal Engineering*, 30(2022), 101805.

[9] Wu, Y., et al., Effect of the Inclination Angle on the Steady-State Heat Transfer Performance of a Thermosyphon[J]. *Applied Sciences*,9(2019), 3324.

[10] Yuan, J., et al., Effect of non-condensable gas on thermal characteristics in two-phase closed thermosyphon[J]. *Applied Thermal Engineering*, 173(2020), 115233.

[11] Fadhl, B., et al., CFD modelling of a two-phase closed thermosyphon charged with R134a and R404a[J]. *Applied Thermal Engineering*, 78(2015), pp. 482-490.

[12] Lu, J., et al., Experimental Study on Heat Transfer Characteristics of Thermosyphon with Methanol-Based Binary Working Fluid[J]. *Iranian Journal of Science and Technology, Transactions of Mechanical Engineering*, 2023, pp. 1-13.

[13] Amatachaya, P., Srimuang, W., Comparative heat transfer characteristics of a flat

two-phase closed thermosyphon (FTPCT) and a conventional two-phase closed thermosyphon (CTPCT)[J]. *International Communications in Heat and Mass Transfer*, 37(2010), pp. 293-298.

[14] Singh, R. R., et al., Effect of anodization on the heat transfer performance of flat thermosyphon[J]. *Experimental Thermal and Fluid Science*, 68(2015), pp. 574-581.

[15] Naresh, Y., Balaji, C., Experimental investigations of heat transfer from an internally finned two phase closed thermosyphon[J]. *Applied Thermal Engineering*, 112(2017), pp. 1658-1666.

[16] Emam, M., et al. Performance improvement of single-junction photovoltaic systems using a new design of a heat pipe-based heat sink: Experimental study[J]. *Applied Thermal Engineering*, 219(2023), 119653.

[17] Hussein., H. M. S., et al., Performance of wickless heat pipe flat plate solar collectors having different pipes cross sections geometries and filling ratios[J]. *Energy Conversion and Management*, 47(2006), pp. 1539-1549.

[18] Tao, J., et al., Experimental study on liquid charging levels of elliptical gravity heat pipes[J]. *Journal of Huazhong University of Science and Technology*, 6(1989), pp. 7-11. (in Chinese language)

[19] Tao, J., et al., Study on the heat transfer characteristics of elliptical gravity heat pipes[J]. *Journal of Huazhong University of Science and Technology*, 3(1990), pp. 39-44. (in Chinese language)

[20] Brackbill, J. U., et al., A continuum method for modeling surface tension[J]. *Journal of Computational Physics*, 100(1992), pp. 335-354.

[21] Su, Z., et al., Investigation of improved VOF method in CFD simulation of sodium heat pipes using a multi-zone modeling method[J]. International Communications in Heat and Mass Transfer 157 (2024), 107669.

[22] Liu, H., et al., An assessment and analysis of phase change models for the simulation of vapor bubble condensation[J]. *International Journal of Heat and Mass Transfer*, 157 (2020), 119924.

[23] Tang, J., et al., A machine-learning based phase change model for simulation of bubble condensation[J]. *International Journal of Heat and Mass Transfer*, 178 (2021), 121620.

[24] Wang, K., et al., Investigation of heat transfer and flow characteristics in two-phase loop thermosyphon by visualization experiments and CFD simulations[J]. International Journal of Heat and Mass Transfer 203 (2023), 123812.

[25] Ding, L., et al., A modified dynamic Lee model for two-phase closed thermosyphon (TPCT) simulation[J]. *Numerical Heat Transfer, Part B: Fundamentals*, 85 (2024), pp. 1041-1055.

[26] Alizadehdakhel, A., et al., CFD modeling of flow and heat transfer in a thermosyphon[J]. *International Communications in Heat and Mass Transfer*, 37(2010), pp. 312-318.

[27] Abdullahi, B., Development and Optimization of heat pipe based Compound Parabolic Collector[D]. University of Birmingham, 2015.

Submitted 13.11.2024.
Revised 21.12.2004.
Accepted 26.12.2024.